JOURNAL OF GEOPHYSICAL RESEARCH, VOL. 113, B08405, doi:10.1029/2008JB005594, 2008

Simultaneous inversion of mantle properties and initial conditions using an adjoint of mantle convection

Lijun Liu[1] and Michael Gurnis[1]

Received 16 January 2008; revised 7 April 2008; accepted 21 April 2008; published 8 August 2008.

[1] Through the assimilation of present-day mantle seismic structure, adjoint methods can be used to constrain the structure of the mantle at earlier times, i.e., mantle initial conditions. However, the application to geophysical problems is restricted through both the high computational expense from repeated iteration between forward and adjoint models and the need to know mantle properties (such as viscosity and the absolute magnitude of temperature or density) a priori. We propose that an optimal first guess to the initial condition can be obtained through a simple backward integration (SBI) of the governing equations, thus lessening the computational expense. Given a model with known mantle properties, we show that a solution based on an SBI-generated first guess has smaller residuals than arbitrary guesses. Mantle viscosity and the effective Rayleigh number are crucial for mantle convection models, neither of which is exactly known. We place additional constraints on these basic mantle properties when the convection-induced dynamic topography on Earth's surface is considered within an adjoint inverse method. Besides assimilating present-day seismic structure as a constraint, we use dynamic topography and its rate of change in an inverse method that allows simultaneous inversion of the absolute upper and lower mantle viscosities, scaling between seismic velocity and thermal anomalies, and initial condition. The theory is derived from the governing equations of mantle convection and validated by synthetic experiments for both one-layer viscosity and two-layer viscosity regionally bounded spherical shells. For the one-layer model, at any instant of time, the magnitude of dynamic topography is controlled by the temperature scaling while the rate of change of topography is controlled by the absolute value of viscosity. For the two-layer case, the rate of change of topography constrains upper mantle viscosity while the magnitude of dynamic topography determines the temperature scaling (lower mantle viscosity) when upper-mantle (lower-mantle) density anomaly dominates the flow field; this two-stage scheme minimizes the tradeoff between temperature and lower mantle viscosity. For both cases, we show that the theory can constrain mantle properties with errors arising through the adjoint recovery of the initial condition; for the two-layer model, this error is manifest as a tradeoff between the temperature scaling and lower mantle viscosity.

Citation: Liu, L., and M. Gurnis (2008), Simultaneous inversion of mantle properties and initial conditions using an adjoint of mantle convection, *J. Geophys. Res.*, *113*, B08405, doi:10.1029/2008JB005594.

1. Introduction

[2] Geophysical observations, especially seismic tomography, plate motions, and the geoid have provided valuable constraints on mantle viscosity and temperature. Global seismic tomography has provided constraints through the resolution of slab-like high-velocity anomalies extending into the lower mantle and large-scale low-velocity anomalies rising from the CMB [*Grand et al.*, 1997; *Van der Hilst et al.*, 1997; *Masters et al.*, 2000; *Ritsema et al.*, 2004]. Deep-rooted columnar low seismic velocity structures, associated with surface hot spots, may have been detected and could be indicative of active mantle plumes [*Montelli et al.*, 2004]. Closer to the surface, regional tomography has imaged active subduction zones showing high seismic velocity slabs overlain by low-velocity mantle wedges [*Zhao et al.*, 1997; *Huang and Zhao*, 2006]. Although tomographic images are informative by providing a snapshot of mantle convection, the observation only constrains the final instant of a time-evolving system. Moreover, we do not know the exact scaling from seismic velocities to either temperature or density.

[3] Other observations beyond seismic imaging and gravity that extend into the time domain are needed to constrain the time dependence. An important constraint comes from the velocity of plates and their time dependence that can be

[1]Seismological Laboratory, California Institute of Technology, Pasadena, California, USA.

0148-0227/08/2008JB005594$09.00

predicted in global flow models [*Lithgow-Bertelloni and Richards*, 1998]. Another possibility comes from surface topography (through stratigraphy and relative sea level) that has been used as constraints on time-dependent models of mantle convection [*Gurnis*, 1993], some with assimilated plate motions [*Gurnis et al.*, 1998]. However, previous models of mantle convection have faced the difficulty of incorporating reasonable initial conditions. For example, *Bunge et al.* [1998] assumed a quasi-steady state mantle structure achieved by imposing the Cretaceous plate motion for a relatively long time before allowing time-dependent plate kinematics to start. This assumption is potentially problematic since plate motions change continuously. *Gurnis et al.* [1998] used an initial condition at 140 Ma in a model of the Australian region based on the earlier geological evolution. *Steinberger and O'Connell* [2000] and *Conrad and Gurnis* [2003] utilized a simple backward integration of the convection equations while neglecting thermal diffusion to predict past mantle structure. This method limits its application, because neglecting thermal diffusion will lead to the accumulation of artifacts at thermal boundaries with time [*Ismail-Zadeh et al.*, 2004].

[4] An alternative approach to recovering initial conditions is through the use of the adjoint method widely used in meteorology and oceanography [*Talagrand and Courtier*, 1987] and recently applied to mantle convection [*Bunge et al.*, 2003; *Ismail-Zadeh et al.*, 2004]. The method constrains the initial condition by minimizing the mismatch of a prediction to observation iteratively in a least squares sense. *Bunge et al.* [2003] implemented an iterative method within a model of spherical-shell mantle convection and explored the method with synthetic experiments; initial conditions were well recovered. Instead of running the adjoint equation for the whole time period in a single iteration, as in the method of *Bunge et al.* [2003], *Ismail-Zadeh et al.* [2004] recovered initial conditions by integrating backward with the forward adjoint looping embedded within each time step. This different iterative scheme was carried out in a fluid with temperature-dependent viscosity within a Cartesian domain. For the problem explored, the forward adjoint looping reduced the total calculation time substantially. The application of these methods to real geophysical problems, however, is limited by the fact that besides the past mantle structures, the rheology and effective Rayleigh number of the mantle are unknown. In other words, in order to restore the structure of the mantle at some point in the past, we first need to have independent constraints on the viscosity and density (or temperature) of the mantle.

[5] In this paper we attempt to overcome this limitation and recast the problem so that mantle temperature and viscosity (effectively, the Rayleigh number) are left as unknowns in addition to the initial condition. In addition to present-day images of the mantle (i.e., from seismic tomography), we add two additional constraints: surface dynamic topography and its rate of change as a function of time. The method is developed and its limitations explored with a suite of synthetic experiments. Using seismic tomography, plate motions, and stratigraphic observations, the method is applied to the descent of the Farallon slab beneath North America since the Cretaceous (L. Liu et al., Reconstructing Farallon plate subduction beneath North America back to the Late Cretaceous, manuscript in review, 2008).

2. Adjoint Method in Mantle Convection

[6] To develop the adjoint method, consider an initial value problem in which all the governing equations and boundary conditions are known and numerical errors are negligible. Any mismatch in the prediction with respect to observation should be attributed to errors in the initial condition. This relation can be expressed as $dJ = (\partial J/\partial \vec{a})d\vec{a}$, where J is a scalar cost function, which defines the mismatch of prediction from data and $\vec{a}$ is the initial variable that potentially carries error. If the expression $\partial J/\partial \vec{a}$ can be obtained, then the perturbation (the error) $d\vec{a}$ of the initial condition can be retrieved. For simplicity, we define the cost function J as a function of temperature T as

$$J = \int_V \left(T_p - T_d\right)^2 dv \tag{1}$$

where T_p is the predicted temperature and T_d is the actual temperature (with the subscript d denoting data).

[7] The governing equations for mantle convection, assuming incompressibility and a Newtonian fluid, are

$$\nabla \cdot \vec{u} = 0 \tag{2}$$

$$\nabla P + \nabla \cdot \left(\eta \nabla \vec{u}\right) = \rho_m \alpha \Delta T \vec{g} \tag{3}$$

$$\frac{\partial T}{\partial t} + \vec{u} \cdot \nabla T = \kappa \nabla^2 T \tag{4}$$

where $\vec{u}$ is velocity, P is dynamic pressure, η is dynamic viscosity, ρ_m is ambient mantle density, α is coefficient of thermal expansion, ΔT is temperature anomaly, $\vec{g}$ is gravitational acceleration, T is temperature, and κ is thermal diffusivity.

[8] We assume that T is the only variable that brings error into our prediction. Our goal is to obtain the expression $\partial J/\partial T$. This expression can be obtained through a constraint on the energy equation by introducing the adjoint variable λ (mathematically the Lagrangian multiplier) that forms a Lagrangian function L [cf. *Sun et al.*, 1991]

$$L = J + \int_V \lambda \left(\frac{\partial T}{\partial t} + \vec{u} \cdot \nabla T - \kappa \nabla^2 T\right) dv \tag{5}$$

[9] A perturbation in L corresponds to perturbations in J and T, respectively. Subsequently, we will use δ to represent perturbed quantities.

$$\delta L = \delta J + \int_V \lambda \left(\frac{\partial \delta T}{\partial t} + \vec{u} \cdot \nabla \delta T - \kappa \nabla^2 \delta T\right) dv \tag{6}$$

[10] In principle, the velocity u should also contribute to this perturbation since it depends on T (see equation (3)), but we choose to neglect the velocity dependence in

Table 1. Summary of Model Parameters

Parameter	Symbol	Value
Radius of the Earth	R_o	6371 km
Gravitational acceleration	g	9.81 m s^{-2}
Reference mantle density	ρ_m	3300 kg m^{-3}
Reference viscosity	η_o	10^{21} Pas
Thermal diffusivity	κ	10^{-6} m^2 s^{-1}
Thermal expansity	α	3×10^{-5}
Superadiabatic temperature drop from CMB to surface	ΔT	393°C (sections 3.1 and 4) 1965°C (section 3.2)

equation (6). This is because, first, a full differentiation of equation (5) leads to a coupled system of the adjoint and forward models which is numerically challenging to implement [*Bunge et al.*, 2003]; second, inaccuracy from omission of the u-dependence in equation (6) is diminished by the variational approach to the single temperature-adjoint solution through iterative schemes we will describe. By applying integration by parts over time and space to equation (6) with appropriate boundary conditions, we obtain an expression of $\delta J/\delta T$

$$\frac{\delta J}{\delta T} = \frac{\partial \lambda}{\partial t} + \vec{u} \cdot \nabla \lambda + \kappa \nabla^2 \lambda \tag{7}$$

This is also called the adjoint equation.

[11] In practice, $\delta J/\delta T$ is nonzero only at the final time for a mantle convection model when the mismatch between prediction and data is made. The adjoint energy equation is the same as the forward energy equation except for the diffusion term that has an opposite sign. This feature enables the adjoint equation to describe the backward advection-diffusion process. This adjoint of the energy equation has been derived for meteorological [*Sun et al.*, 1991; *Sirkes and Tziperman*, 1997] and mantle convection problems [*Bunge et al.*, 2003; *Ismail-Zadeh et al.*, 2004].

[12] We interleaved the backward adjoint calculation with a forward solution of the energy and momentum equations within an iterative procedure similar to that proposed by *Bunge et al.* [2003]. Our convention for subscript refers to time (0 for initial; 1 for present) while those for superscripts refer to the number of iterations. The number of iterations is determined by the accuracy to which we desire our prediction to satisfy data. Specifically, these are the steps followed:

[13] 1. Solve the forward problem with all three governing equations (equations (2) to (4)) with initial condition T_0^n ($0 \le n \le N$, where n is the iteration number) and predict T_1^n. The first initial condition T_0^0 is potentially arbitrary. Store the velocity field for all time steps.

[14] 2. Compute the mismatch J^n and its gradient $\partial J^n/\partial T_1^n$; solve the adjoint energy equation (equation (7)) with the velocity stored in step 1 from t_1 to t_0 and obtain λ_0^n.

[15] 3. Update the initial field: $T_0^{n+1} = T_0^n - \alpha(n) \cdot \lambda_0^n$, where $\alpha(n)$ is a damping factor (defined as in the work of *Ismail-Zadeh et al.* [2004] except that we took a simple form assuming $\alpha(n)$ only depends on n), with n_0 an adjustable integer

$$\alpha(n) = 1/(n + n_0) \tag{8}$$

[16] For each experiment described below, we assume that the true mantle temperature in both the past and present are known. This past mantle state is the solution we seek by applying the adjoint method, and the present state is the target function we match with the prediction. These so-called reference states are generated by forward runs solving the normal convection equations (equation (2)–(4)).

[17] The forward and adjoint models, as described above, were computed with *CitcomS*, a finite element code that solves thermal convection problems relevant to Earth's mantle [*Zhong et al.*, 2000; *Tan et al.*, 2006]. The version of *CitcomS* used here solves the equations in a spherical geometry and scales well on large parallel computers. Our changes were made to *CitcomS* version 2.1.0 obtained from the Computational Infrastructure for Geodynamics (http://geodynamics.org).

[18] Our first goal is to find an optimal implementation of the adjoint method as presented in section 2, reducing the computational cost while reasonably solving for the initial condition. To start the iteration, the adjoint method requires a first guess to the initial condition. For a linear inverse problem, the solution is independent of the first guess [*Tarantola*, 2005]. However, mantle convection is a nonlinear problem and the adjoint method is applied to the energy equation only. This means the solution to the inverse problem may not be independent of the first guess, at least after a reasonable number of iterations.

[19] The model domain is colatitude $\theta \in [1.27, 1.87]$, longitude $\varphi \in [0.0, 0.6]$ (both in radians), and the nondimensional radius $r \in [0.55, 1]$ (normalized by radius of the earth). Boundary conditions for the forward model are: $\vec{n} \cdot \vec{u} = 0$ and $\vec{n} \cdot \nabla \vec{u}_{tg} = 0$ on all boundaries, where $\vec{n}$ is the outer normal vector, $\vec{u}$ is velocity vector, and $\vec{u}_{tg}$ is the tangential velocity; the surface and core-mantle boundary (CMB) are isothermal, while the sidewalls have zero heat flux, i.e., $\vec{n} \cdot \nabla T = 0$. The adjoint model has zero adjoint temperature on the surface and CMB, and zero adjoint heat flux on the sidewalls. In our numerical experiments, the Rayleigh number is defined as

$$Ra = \frac{\rho_m g \alpha R_o^3 \Delta T}{\eta_o \kappa} \tag{9}$$

where ΔT is the temperature drop from CMB to surface. And the actual time t is related to the model time t' by

$$t = t' R_o^2/\kappa \tag{10}$$

[20] All the symbols are listed in Table 1, with their dimensional values. Hereafter in section 3, all physical quantities are normalized with their dimensional values, if not noted separately.

3. Adjoint Models

[21] We carried out two sets of numerical experiments that used the forward adjoint looping to estimate initial conditions. The first set has a uniform viscosity ($\eta = 1$), a constant ambient mantle temperature, and a Rayleigh number of 1.0×10^8. The second set of experiments has a more

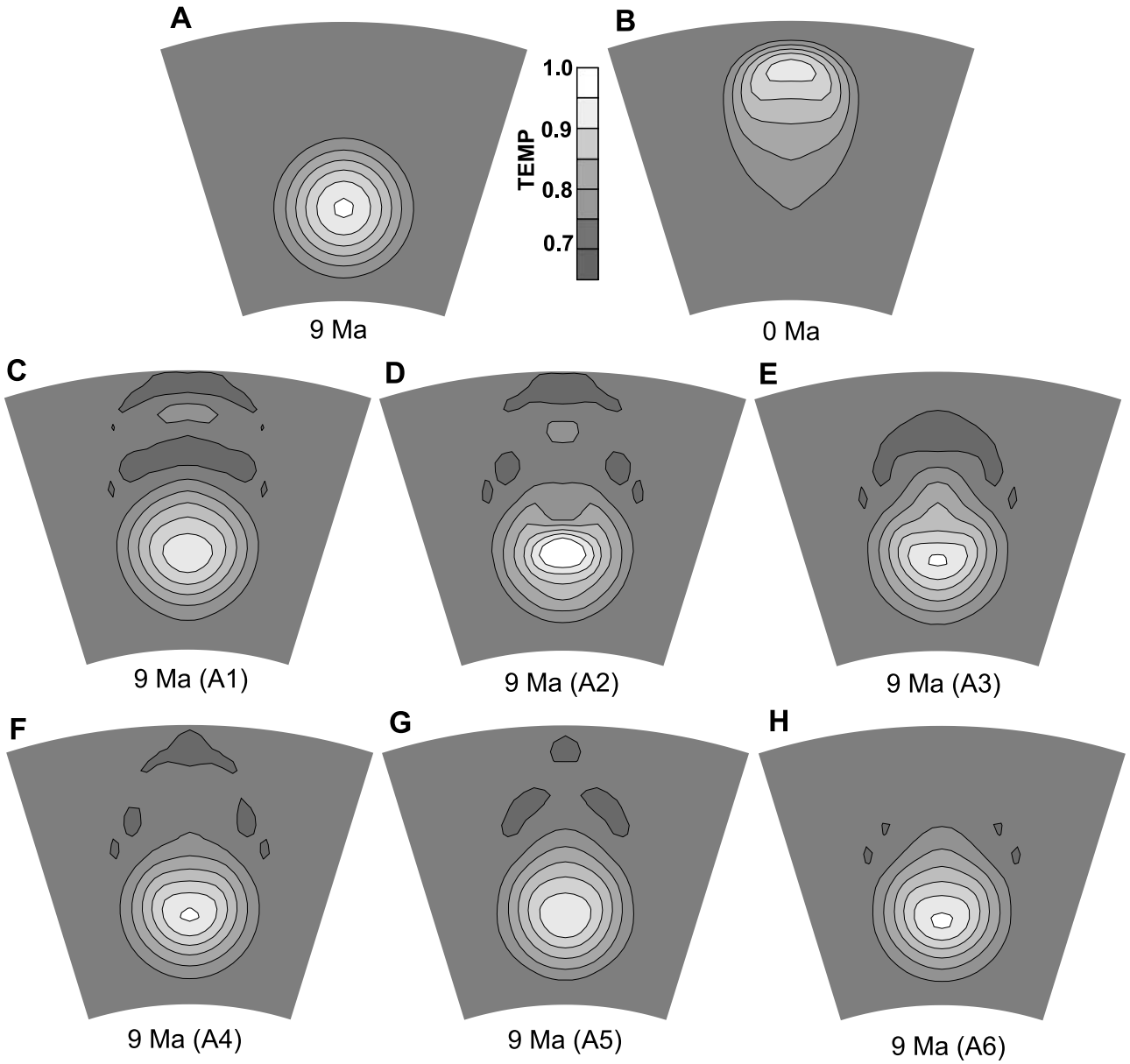

Figure 1. Three-dimension forward-adjoint models (with a 33 × 33 × 33 mesh) for a mantle with a single layer viscosity and uniform background temperature. Shown is temperature for vertical cross sections along lines of latitude through center of the domain. Reference thermal states at (a) 9 Ma and (b) present. (c to h) Retrieved initial states at 9 Ma using 6 different initial guesses (case A1–A6, Table 2). For all cases, 50 forward adjoint iterations were used.

complex viscosity, a thermal boundary layer on top and a higher Rayleigh number.

3.1. Models With a Single Layer

[22] In this first set of experiments, the reference states include an initial condition (Figure 1a) which has a spherical hot anomaly in the lower part of mantle (with a maximum temperature increase of $\Delta T = 0.3$ at the center and a Gaussian temperature profile across the center) and a final condition produced by running the forward model for 9 Ma (Figure 1b). These two reference states are also the targets we try to predict with the adjoint method. All models are computed on a 33 × 33 × 33 grid. We assumed $n_0 = 1$ in equation (8), for the forward adjoint looping.

[23] For this set of experiments, we started the iteration with different first guesses to the target initial condition (each of these guesses constituted different cases, A1–A6, with "A" denoting adjoint method). Either we assumed a uniform temperature, a temperature that was a function of the actual initial condition, or generated an estimate through a simple backward integration (SBI) of the governing equations. The SBI was obtained by reversing the sign of gravity from the forward calculation and integrating from t_1 to t_0. The initial guesses were arranged in order of how close they are to the target initial condition (Table 2). Specifically, case A1 had a nearly isothermal condition with a tiny perturbation. Case A2 had an anomaly with the same

Table 2. Description of the Thermal Anomaly Structures in the Reference Initial State and Various First Guesses

	Geometry	Center (θ, ϕ, r)	Diameter[a] (dimensionless)	Magnitude (ΔT)
Reference	sphere	(1.57, 0.3, 0.7)	0.3	0.3
Case A1	sphere	(1.57, 0.3, 0.7)	0.3	0.001
Case A2	sphere	(1.57, 0.3, 0.7)	0.15	0.5
Case A3	sphere	(1.57, 0.3, 0.78)	0.3	0.3
Case A4	sphere	(1.57, 0.39, 0.7)	0.3	0.3
Case A5	sphere	(1.57, 0.3, 0.7)	0.4	0.3
Case A6	SBI[b]	-	-	-

[a]Diameter of the spherical anomaly, normalized by R_o, radius of the Earth.

[b]Note that SBI means simple backward integration, i.e., reverse the sign of gravity and run the forward model from the present-day mantle structure for the same amount of time.

center as the target, but with a smaller volume (1/8×) and buoyancy. Cases A3 had the same shape and buoyancy compared to the target, but the center was shifted upward by 500 km. Case A4 also had the same shape and buoyancy as the target but its center was shifted horizontally by 400 km. Case A5 had the same center but the anomaly had a larger volume (2.4×) and buoyancy. Case A6 used the SBI to obtain the first guess.

[24] For comparison, we ran all cases for 50 iterations while tracking the recovered initial conditions. These retrieved initial conditions were noticeably different, and the recoveries in cases A4 to A6 (Figures 1f–1h) were better than those in A1 to A3 (Figures 1c–1e). Case A6 gave the best recovery (Figure 1h). The root mean square (RMS) residuals between the recovered initial conditions and the target initial (Figure 2a), and those between the predicted and target final (Figure 2b) decreased with the number of iterations. The terminal (at n = 50) residuals for both the initial and final states (Figures 2a and 2b), decreased from case A1 to A6 as the first guess more closely reflected the target initial condition. The SBI (A6), especially, started the first iteration with residuals far smaller than the others and the residuals with the final state remained small in comparison to the other cases (Figures 2a and 2b). The rate of convergence was also dependent on the initial guess: the closer the first guess to the target initial condition, the faster the convergence (Figures 2a and 2b). The SBI was one of the fastest converging cases and required the least number of iterations to converge. If the final solution is achieved when the slope of the residual between predicted and target final decreases to below a specified small value, then solving for the initial condition with the SBI is almost an order of magnitude faster than the others. The convergence of case A1, with the nearly isothermal initial condition is far smaller than A6 using the SBI and much of this difference arises from the organization of the forward adjoint looping. For case A1, the adjoint temperature at t_1 is nearly the negative of the final temperature, in other words, almost possessing the same buoyancy used in the strict reverse calculation (SBI). However, when the adjoint temperature in A1 is advected from t1 to t0, the stored velocity field from the forward calculation is used, but this velocity field is quite different from the actual. The SBI overcomes this limitation by using the velocity field from the actual backward calculation.

[25] Since the solutions are dependent on the first guess, finding the optimal one is important to decrease calculation time while obtaining a reasonable solution. Because the SBI gives the best solution to the initial condition, both in terms of the terminal residual and the rate of convergence, we consider this to be a useful means to obtain an optimal first guess. Another advantage of obtaining the first guess via the SBI is that it requires no a priori information of the solution. Algorithmically, it is also easy to obtain.

3.2. Models With Thermal Boundary Layers and Depth- and Temperature-Dependent Viscosities

[26] The second set of experiments is geophysically more realistic with a top thermal boundary layer (TBL) representing the lithosphere and a four-layer mantle with temperature-dependent viscosity. The TBL has an error function temperature profile typical of a 40 Ma oceanic lithosphere. The viscosities for lithosphere, upper mantle, transition zone, and the lower mantle, without temperature-dependence, are 10, 1, 10, and 40, respectively. The temperature-dependence on viscosity is given by

$$\eta_T = \eta_o \times \exp\left(\frac{1}{T+0.3} - 1\right) \tag{11}$$

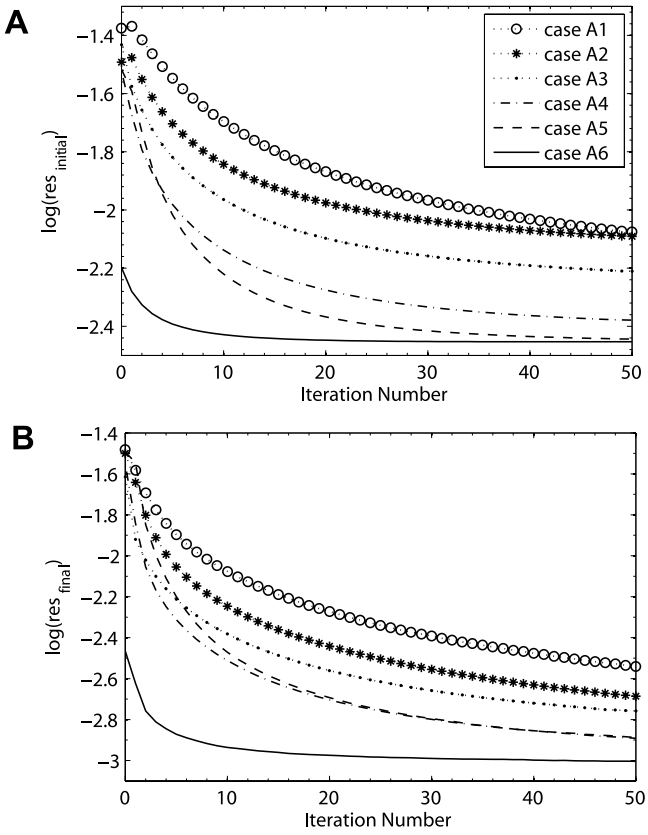

Figure 2. Convergence of the models shown in Figure 1. (a) Root mean square (RMS) residuals of recovered initial conditions with respect to the reference initial versus iteration. (b) RMS residuals of the predicted final conditions with respect to the reference final versus iteration.

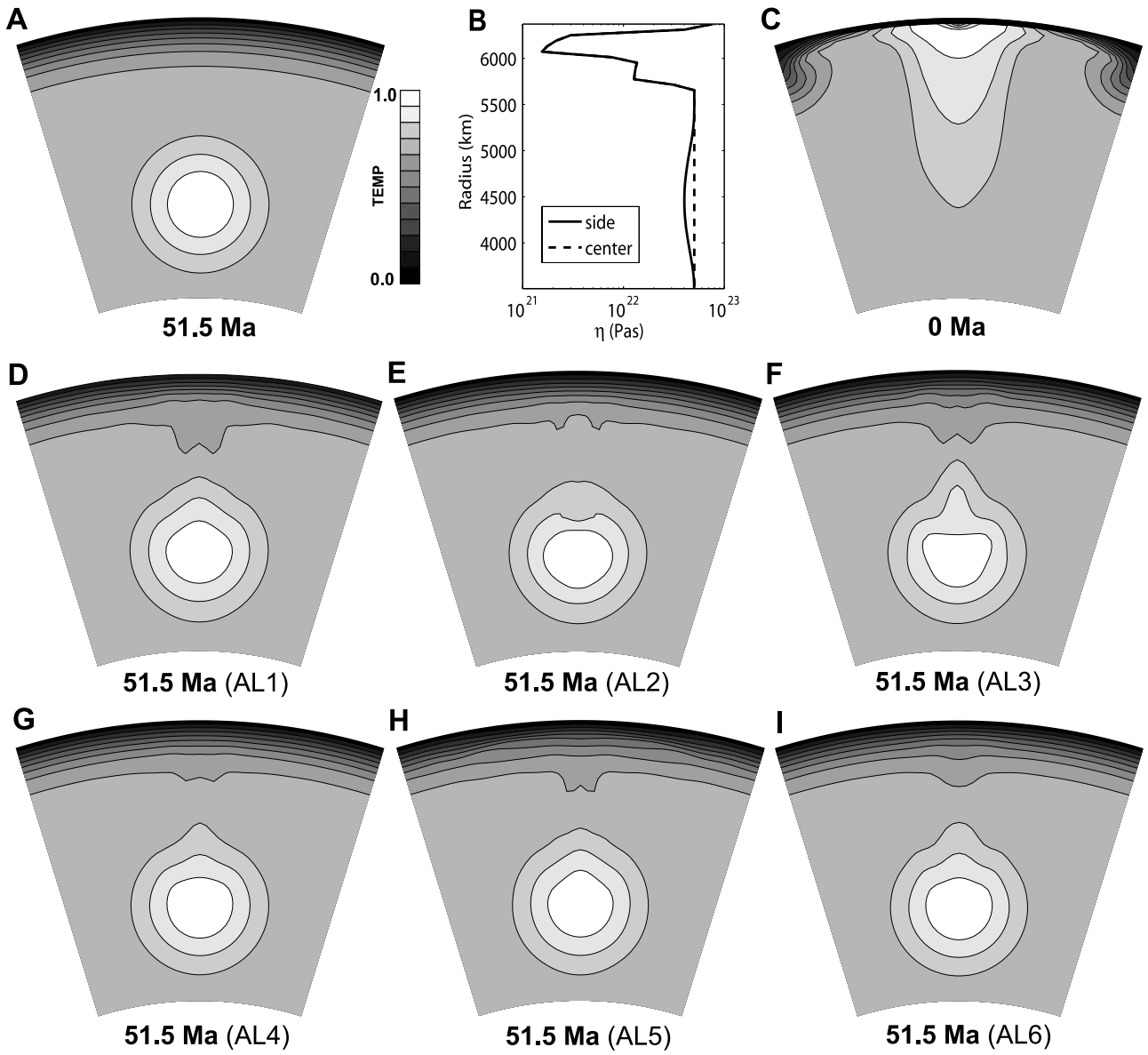

Figure 3. Three-dimension forward adjoint models (with a 49 × 49 × 49 mesh) for a model with a radially stratified viscosity and a top thermal boundary layer. Shown is temperature through vertical cross sections. Reference states at (a) 51.5 Ma and (c) present. (b) Radial viscosity profiles in the reference initial condition. (d to i) Retrieved initial states from 6 different initial guesses (AL1–AL6) after 50 iterations.

where η_T is temperature-dependent viscosity and η_o temperature-free viscosity. This results in an order of magnitude decrease in viscosity from $T = 0$ to 1. We also used a higher Rayleigh number at 5.0×10^8.

[27] The target initial condition has the same thermal anomaly as that in section 3.1, only that it has a TBL on top (Figure 3a). The target final condition (Figure 3b) is 52 Ma after the anomaly had risen through the upper mantle and eroded the lithosphere. We named six different cases as AL1 to AL6 (L denoting lithosphere). The first guesses in cases AL1 to AL5 had the same anomaly structures as described in Table 2, and they all had the same TBL as in the target initial. Case A6 is the SBI. Comparatively, these first guesses in AL1-AL5 had more information on the target initial than those in A1–A5, because we assumed the correct TBL in these guess. On the other hand, case AL6 (using the SBI) had less information on the initial condition because the TBL had to be entirely recovered with the forward adjoint looping. All models were realized with a 49 × 49 × 49 mesh with an underresolved lithosphere spanned with just two mesh points.

[28] Since these models are more complex, and thus more nonlinear, than models in section 3.1, we adopted smaller damping factors α with $n_o = 2$, in order to avoid overcorrection in the iterative process. We integrated the forward and adjoint equations for 50 iterations to obtain the sol-

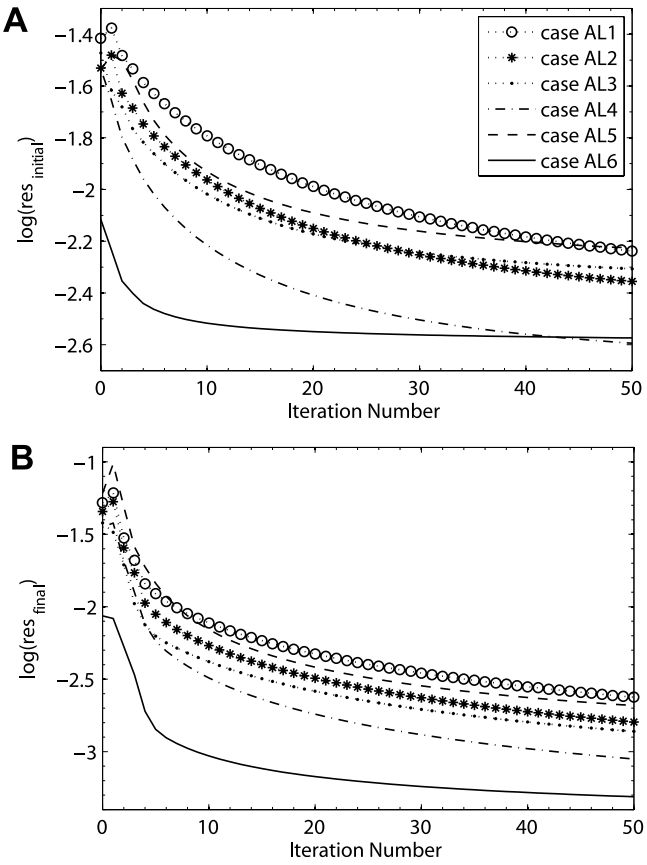

Figure 4. Same as Figure 2 except for the models shown in Figure 3.

utions (Figures 3c–3h). Since the temperature field includes a TBL and a lower mantle anomaly, a small residual would entail recovering both well. The comparison of recoveries in these cases is not as obvious as that of only a rising Stokes sphere (section 3.1). Case AL5 with the closest initial guess also accumulated substantial errors through the nonlinear interaction between the rising spherical anomaly and the thermal erosion of the lithosphere. Case AL4 and AL6 both gave good recoveries with the smallest residuals between recovered and target initial condition (Figure 4a) and that AL6 among all cases had smallest residual between predict and target final condition (Figure 4b). The SBI (AL6) also led to fastest convergence, and most of the residuals were reduced within the first 10 iterations. From both the residuals and rate of convergence, we concluded that the SBI is still the best initial guess even in such a complex model.

[29] Other experiments showed that by increasing n_o, hence decreasing α, we could decrease the terminal residuals of the initial condition in AL1 to AL5 upon convergence, some of which (AL4 and AL5) could be even smaller than in AL6, indicating a better recovery, but the terminal residual of the final condition in AL6 was always the smallest. However, for these tests, we had to increase the number of iterations to obtain the same amount of reduction of residuals; in other words, we reduced the rate of convergence substantially in A1 to A5, while A6 always had the fastest convergence and smallest residuals during most of the iterations. This indicates that the SBI first guess always produces good solutions with least calculation.

4. Incorporation of a Dynamic Topography Constraint

[30] Unlike atmospheric or oceanographic problems where many parameters within the interior of the flow can be measured and calibrated in situ, for the mantle convection problem dynamic parameters are obtained indirectly. A good example of such a parameter is the depth-dependence of mantle viscosity, unfortunately a parameter that remains uncertain [*Walcott*, 1973; *Hager and Clayton*, 1988; *Steinberger and O'Connell*, 2000; *Mitrovica and Forte*, 2004]. This of course is problematic for the adjoint problem described in section 3 or in the work of *Bunge et al.* [2003] or *Ismail-Zadeh et al.* [2004], because what viscosity should be used for the recovery of initial conditions? Another critical parameter for such recoveries is the magnitude of the temperature or density anomalies. Clearly, important constraints can be placed on this problem from seismic tomography, but high-pressure high-temperature laboratory experiments have not achieved the ability to uniquely map seismic into thermal anomalies. Thus, even for simple convection models, we should consider these basic model parameters to have uncertainty when the adjoint method is used to infer initial conditions.

[31] With the adjoint method implemented in *CitcomS*, we can compute the prior history of thermal anomalies for a given viscosity model and present-day mantle thermal structure. From the restored history, we then predict dynamic topography that can be constrained through stratigraphic constraints, such as tectonic subsidence from boreholes [*Pang and Nummedal*, 1995], paleoshorelines [*Bond*, 1979; *Sandiford*, 2007; L. DiCaprio et al., Long-wavelength tilting of the Australian continent since the Late Cretaceous, submitted to *Earth and Planetary Science Letters*, 2008], and sediment isopachs [*Cross and Pilger*, 1978]. Given these additional observational constraints, there is the opportunity to place limits on mantle viscosity and temperatures.

4.1. Isoviscous Mantle

[32] First let us consider a mantle with a uniform viscosity throughout. On the top surface of the convection model, dynamic topography, h, is defined from

$$\sigma_{r,r} = \rho_m g h \tag{12}$$

where $\sigma_{r,r}$ is the total normal stress in the radial direction and ρ_m is the density contrast across the top surface (implicitly assuming that air overlies the solid mantle). At any instant of time, normal stress $\sigma_{r,r}$ is proportional to the temperature scaling ΔT (see equation (3)). For an inverse problem where we use the present-day seismic tomography to interpret mantle temperature structure, ΔT is the temperature magnitude obtained by mapping seismic velocity variations to thermal anomalies. Together with equation (12), we relate dynamic topography with a temperature scaling via a time-dependent coefficient ζ with units, *m/K*. The quantity ζ describes the response of surface

dynamic topography with a scaled temperature distribution and mantle rheology structure.

$$h(t) = \zeta(t)\Delta T \tag{13}$$

[33] The rate of change of dynamic topography $\dot{h}$, however, is related to the absolute viscosity of the mantle when the geometry of the thermal anomaly remains fixed [*Gurnis et al.*, 2000]. Specifically, in the energy equation (equation (4)), the rate of change of the temperature anomaly ΔT is proportional to the product of ΔT and mantle flow speed $\vec{u}$ (i.e.$\Delta\dot{T} \propto \vec{u} \cdot \Delta T$). In a Stokes fluid, $\vec{u}$ is proportional to ΔT and inversely proportional to mantle viscosity η. Considering equation (13), we obtain

$$\dot{h}(t) = \frac{\xi'(t)}{\eta}\Delta T^2 \tag{14}$$

[34] For an inverse problem where ΔT and η are unknowns, and $h(t)$ and $\dot{h}(t)$ are data constraints, we simplify the problem by rewriting equation (14) with equation (13)

$$\dot{h}(t) = \frac{\xi(t)}{\eta}h_1^2 \tag{15}$$

where $h_1 = h(t_1)$, with t_1 representing present-day time; ξ (or ξ') is a kernel that describes the response of the rate of change of surface dynamic topography assuming a specific mantle viscosity; ξ has units of *Pa/m*. Instantaneously, when the temperature and viscosity structures remained unchanged, equation (15) was validated numerically for systems with temperature- and depth-dependent viscosities [*Gurnis et al.*, 2000].

[35] Because $h(t)$ and $\dot{h}(t)$ are potentially two independent constraints, and equations (13) and (15) each have an independent unknown, ΔT and η, respectively, the independent unknowns might be recoverable. By using h_1 instead of $h(t)$ on the right hand side of equation (14), we attempt to partially decouple this two-variable, two-constraint system. Essentially, we use the magnitude of topography $h(t)$ to constrain ΔT (equation (13)), and use its rate of change $\dot{h}(t)$ to constrain η(equation (15)).

[36] The left-hand sides of equations (13) and (15) are time-dependent. On the right-hand side of the equations, the time dependence has been collapsed into the two kernels, ζ and ξ, which are evaluated numerically. At any moment of time, ζ and ξ can be found from the solution of equation (2)–(4) and are dependent on the viscosity and temperature distribution. Evaluation of ξ requires two successive solutions of equation (2)–(4) so that $\dot{h}(t)$ can be found.

[37] Assuming the "structure" of the present-day temperature field is the same as the structure obtained from seismic tomography, we now show how equation (13) and equation (15) can be incorporated within an iterative scheme to solve for the unknowns ΔT and η based on observed and predicted $h(t)$ and $\dot{h}(t)$. Define j to be the index of a loop used to refine temperature and viscosity, while i remains the index over time as it was in the forward adjoint looping (section 3). At any given time i in loop j, the numerical values of the two kernels ζ and ξ are computed as $\zeta_{ij} = h_i/\Delta T^j$, $\xi_{ij} = \dot{h}_i \cdot \eta^j/(h_1)^2$, respectively. Here we treat two kernels as implicit Green's functions. ΔT and η are updated by a method that is similar to back-projection used in seismic topography [*Rowlinson and Sambridge*, 2003], the difference being the use of implicit coefficients (ζ and ξ) in this case.

$$\Delta T^{j+1} = \Delta T^j + \frac{\gamma_1}{n}\sum_{i=1}^{n}\zeta_{ij}[h_{d_i} - h_i] \tag{16}$$

$$\eta^{j+1} = \eta^j + \frac{\gamma_2}{m}\sum_{i=1}^{m}\xi_{ij}\left[\frac{h_{d1}^2}{\dot{h}_{d_i}} - \frac{h_1^2}{\dot{h}_i}\right] \tag{17}$$

where m and n are the numbers of sample points within the time series and are potentially different because of the different number of constraints on topography and its rate of change; subscript d refers to data (observational constraints); γ_1 and γ_2 are two damping factors with values $<= 0.5$.

[38] This iteration is at a higher level than that of forward adjoint looping and we refer to it as the outer iteration. Essentially, seismic tomography at the present-day is used to constrain the geometry or depth distribution but not the precise amplitude of mantle temperature anomalies, and the forward adjoint looping is used to find that geometry during earlier times. The outer looping is used to refine both the scaling between seismic velocity variations and temperatures (or density) and the viscosity distribution. The whole procedure is divided into two parts:

[39] 1. The first part is the inner loop. While ΔT and η (without varying temperature-dependence) remain constant, perform adjoint calculation to recover the initial condition with the SBI first guess, and predict the dynamic topography during the final iteration.

[40] 2. The second part is the outer loop. Update ΔT and η via (16) and (17) through the mismatch of the predicted and target dynamic topography and its rate of change.

[41] The whole procedure is terminated upon convergence of the two model parameters.

[42] In a synthetic experiment, a cold spherical anomaly sinks from top to bottom of the mantle within a 3-D spherical region; the system has initial (Figure 5a) and final reference states (Figure 5b). On the top surface, topography is sampled directly above the center of the anomaly. To illustrate the effect of forward adjoint iteration on dynamic topography, we ran the inner loop described above assuming that the temperature scaling and the absolute value of viscosity are known. The SBI initial guess (Figure 5c) is more diffused in comparison to the finally recovered initial condition after 50 iterations (Figure 5d). The adjoint method reduces the RMS residuals for the initial and final states by about a factor of 3 and 5, respectively (Figure 5e). Consequently, the associated dynamic topography curves from t_0 to t_1 are also notably different (Figure 5f). The curve from the SBI deviates from the reference much more than the one from the recovered solution, with a maximum deviation in magnitude by 35% versus 5% of the reference value at 16 Ma. Although the SBI is a good method to find the best

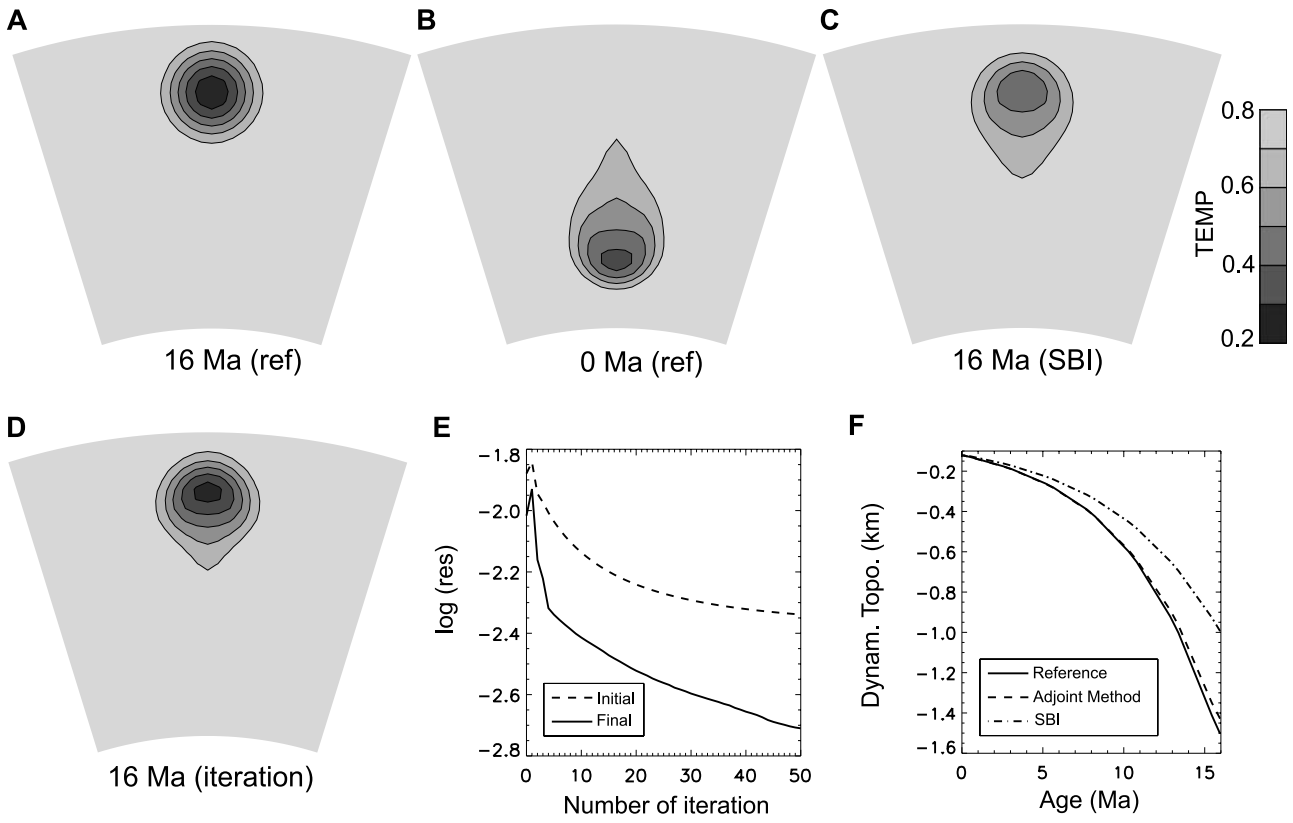

Figure 5. Three-dimensional model with a single viscosity layer (modeled with a 33 × 33 × 33 mesh). Reference thermal states at (a) 16 Ma and (b) the present. (c) First guessed initial condition with a simple backward integration (SBI). (d) Recovered initial condition with the adjoint method after 50 iterations. (e) RMS residuals for the initial and final states based on the adjoint method. (f) The predicted dynamic topography histories based on SBI and the adjoint method, compared against the reference dynamic topography. All calculations assume a known viscosity structure.

first guess for the forward adjoint looping, the experiment demonstrates that the simple backward advection of the anomaly (SBI) does not perfectly predict the evolution of dynamic topography.

[43] We then started the outer loop with two initial models (cases AH1 and AH2) in which the temperature scaling ΔT and mantle viscosity η had "guessed values" that were different from the reference ones. The initially guessed parameters of case AH1 (Figures 6a and 6b at loop 1) were such that its effective Rayleigh number was equal to the actual *Ra* for the reference state while case AH2 (Figures 6e and 6f at loop 1) had an effective Rayleigh number 4 times smaller. In both cases, we applied the two-level looping algorithm. The inner loop was applied so that the iteration always started with the SBI first guess, and the number of forward adjoint iterations increased as the index of the outer loop increased. We applied this simplification because the first recovered initial condition was not well known before the constraints on *h(t)* and $\dot{h}(t)$ were applied. Owing to the initially underestimated temperature scaling ΔT in both AH1 and AH2, the first predicted temporal dynamic topography curves had small magnitudes and slopes. By applying the outer loop upon the predicted and reference dynamic topography (Figures 6c and 6g), we updated model parameters ΔT and η. The difference in magnitudes of topography *h(t)* forced ΔT to increase in both cases where AH2 increased faster due to a larger difference. Differences in slope $\dot{h}(t)$ normalized by present-day magnitude of topography h_1 updated the viscosity. The apparently smaller slope in AH1 was actually larger than that of the reference when normalized by h_1 and hence forced the viscosity to increase. The initial smaller slope for dynamic topography in AH2 forced the viscosity to decrease, and the smaller magnitude forced temperature to increase, overshooting the reference temperature. The overshot was corrected as the viscosity also approached the true value. As a result, for both cases AH1 and AH2, the temporal (Figures 6c and 6g) and spatial (Figures 6d and 6h) distribution of dynamic topography converged to the target curves as the two incorrectly guessed model parameters converged to the reference values after a finite number of loops (Figures 6a, 6b, 6e, and 6f). Most of the model corrections occurred within the first 10 outer loops.

[44] As discussed in section 3, due to the artificially defined initial condition and low resolution of meshing, the recovered initial condition by the adjoint method is not exact, even with the same model that generates the reference states (Figure 5d). This effect shows up in the recovered model parameters as a deviation of viscosity from the reference value by about −2% and that of the temperature scaling by about 1%. However, the final solutions in both cases AH1 and AH2 are almost identical, indicating the

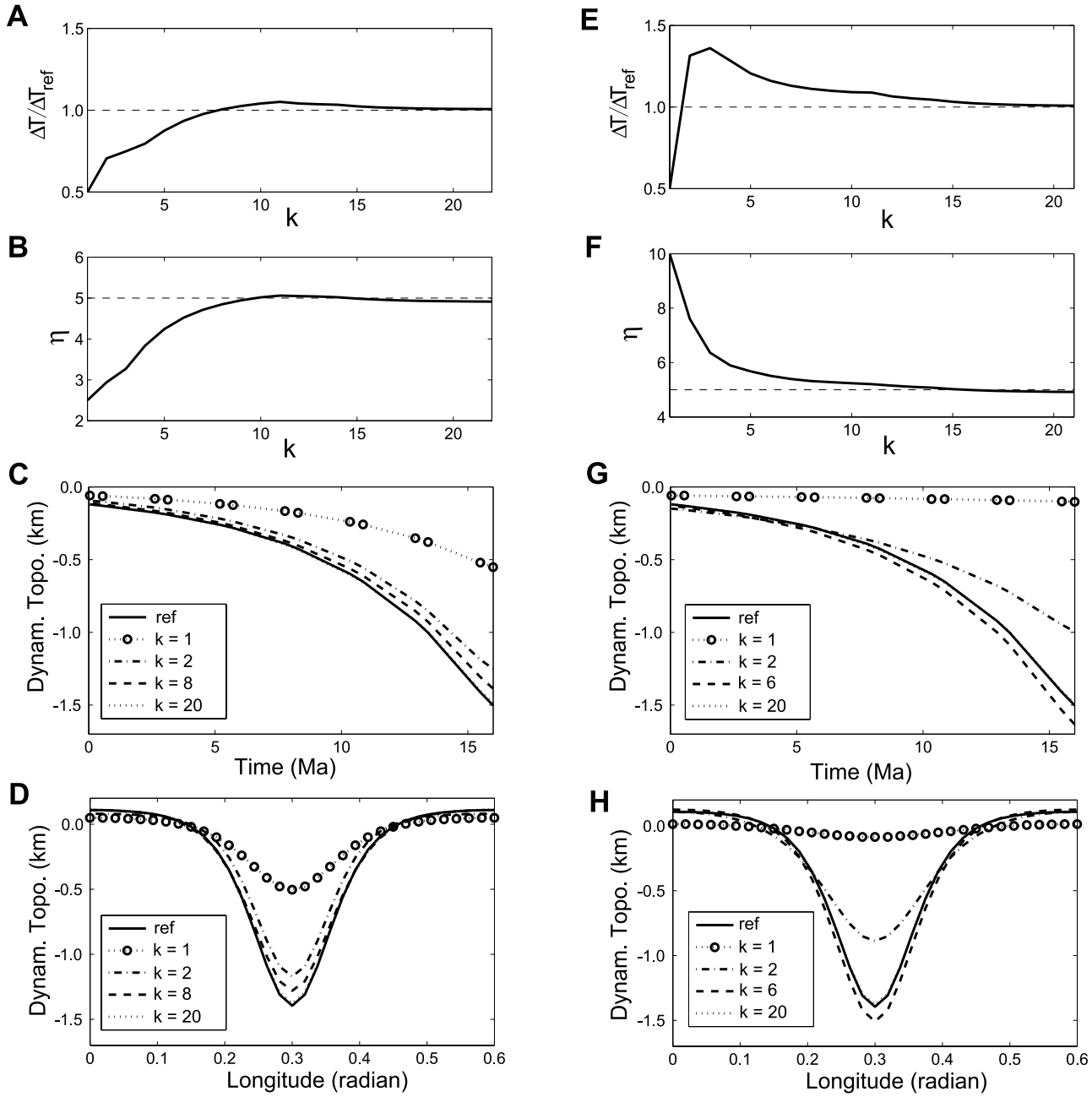

Figure 6. Recovery of model parameters using dynamic topography for models with a single layer. The starting model has either (a–d) the same effective Rayleigh number (case AH1) or (e–h) a Rayleigh number 4 times smaller (case AH2) than the reference value. All results plotted with respect to the outer loop index (k) and are computed from the last iteration of the inner (forward adjoint) looping. Shown from top to bottom are the temperature scaling (Figures 6a and 6e), viscosity (Figures 6b and 6f), temporal evolution of dynamic topography recorded at one point on the surface (Figures 6c and 6g), and latitudinal profile of dynamic topography across the center of the surface at 16 Ma (Figures 6d and 6h).

two-level algorithm can both recover initial conditions and unknown material properties.

[45] Under highly controlled set of circumstances, this test shows that the history of the dynamic topography is a valuable constraint on mantle viscosity and magnitude of present-day mantle thermal structures. We will now explore the limitations of this conclusion under more realistic conditions.

4.2. Layered Mantle

[46] We now consider the geophysically more relevant possibility of a layered mantle viscosity [*Hager*, 1984; *Mitrovica and Forte*, 1997]. We used a two-layer mantle and attempted to recover three variables: ΔT (present-day temperature anomaly), η_{um} (upper mantle viscosity), and η_{lm} (lower mantle viscosity). Given this potentially underdeter-

mined problem, we determine what we might hope to recover.

[47] For a thermal anomaly within the upper mantle, the upper mantle viscosity controls the flow velocity, $\vec{u}$, and the evolving dynamic topography. Assuming that the density anomaly has not yet entered the lower mantle the system has only two variables, ΔT and η_{um}, just like the isoviscous mantle discussed above. This assumption is not entirely true since the h does depend on the ratio of upper to lower mantle viscosity [*Richards and Hager*, 1984; *Hager*, 1984]. Approximately, we still have the linear relation between $\dot{h}(t)$ and ΔT, equation (13), and the following relation for $\dot{h}(t)$, which is similar to equation (14)

$$\dot{h}(t) \approx \frac{\xi'(t)}{\eta_{um}} \Delta T^2 \tag{18}$$

[48] For a density anomaly within the lower mantle, the flow speed $\vec{u}$ is approximately inversely proportional to η_{lm}, and the surface normal stress which defines $h(t)$ is proportional to η_{um}. So equation (13) becomes

$$h(t) = \zeta(t) R_\eta \Delta T \tag{19}$$

where $R_\eta = \eta_{um}/\eta_{lm}$, is the ratio of upper to lower mantle viscosity. Consider a static situation in which we neglect time dependence, equation (19) is nonlinear due to the fact that $\zeta = \zeta(R_\eta)$, while equation (13) is linear since ζ is not a function of ΔT. This implies the inverse problem for a two-layer viscosity mantle is more nonlinear than for a single layer mantle. The relation $\Delta \dot{T} \propto \vec{u} \cdot \Delta T$, together with equation (19), leads to the expression

$$\dot{h}(t) = \frac{\xi(t)}{\eta_{um}} h_1^2 \tag{20}$$

where h_1 is dynamic topography at the present-day. Again, we use h_1 instead of $h(t)$ on the right-hand side of equation (20) to avoid the sharing of data constraints. In fact, equation (18) and (20) are equivalent: replace ΔT with h_1 in equation (18) and equation (20) is obtained. This shows that the rate of change of dynamic topography should be a good constraint on the upper mantle viscosity.

[49] Rearranging and discretizing equation (20) lead to

$$\eta_{um}^{j+1} = \eta_{um}^{j} + \frac{\gamma_3}{m} \sum_{i=1}^{m} v_i \xi_{ij} \left[\frac{h_{D1}^2}{\dot{h}_{Di}} - \frac{h_1^2}{\dot{h}_i} \right] \tag{21}$$

For the other two variables, ΔT and η_{lm}, we have constraint equations (13) and (19). Ideally, we could use equation (13) to constrain ΔT by assimilating topographic data associated with density anomalies crossing the upper mantle through equation (16). Equation (19) could be used to constrain η_{lm} by topographic data with lower mantle anomalies iteratively

$$\eta_{lm}^{j+1} = \eta_{lm}^{j} + \frac{\gamma_4}{l} \sum_{i=1}^{l} w_i \frac{\Delta T^{j+1} \eta_{um}^{j+1}}{\varsigma_{ij}} \left[\frac{1}{h_{Di}} - \frac{1}{h_i} \right] \tag{22}$$

[50] In equations (21) and (22), m and l are the numbers of sample points within the time series; γ_3 and γ_4 are two damping factors with values <= 0.5; two kernels $\zeta_{ij} = R_\eta^j \Delta T^j / h_i$ and $\xi_{ij} = \dot{h}_i \cdot \eta^j / (h_1)^2$; v_i and w_i are weighting functions that change with time. We assumed that v_i (w_i) decreases (increases) linearly from $i = 1$ to l.

[51] However, because a thermal anomaly will move faster in the upper mantle than in the lower mantle, a topographic history would be more heavily weighted in time for the lower mantle, where ΔT largely trades off with η_{lm} when using the dynamic topography (see equation (19)). In other words, temperature anomaly and lower mantle viscosity are coupled for most of the topographic record.

[52] Therefore, in order to simultaneously invert for all three variables, we should avoid the tradeoff between temperature scaling and lower mantle viscosity. We designed a three-level iterative scheme which solves for all three parameters while minimizing potential tradeoffs between them:

[53] 1. The first level is the inner level. While ΔT, η_{um} and η_{lm} remain fixed, perform forward-adjoint looping to recover the initial condition.

[54] 2. The second level is the middle level. While ΔT remains fixed, update η_{um} and η_{lm} via equations (21) and (22) through the mismatch of the predicted and target dynamic topography and its rate of change.

[55] 3. The third level is the outer level. Update ΔT according to equation (16).

[56] The whole procedure is terminated upon convergence of the three model parameters.

[57] For an explicit example, we consider a 2-D model that simulates a subduction scenario, where a fragment of a cold slab sinks from the upper mantle into the low mantle over a period of 36 Ma (Figures 7a and 7b). The dynamic topography is recorded at the surface at some point on the "overriding" plate. We assume that the top surface is fixed; if the plates are moving then the observational record of topography is in the plate frame [*Gurnis et al.*, 1998] and using the mismatch between observed and predicted quantities will be more involved than what the experiment given below suggests.

[58] To avoid numerical artifacts, we generated the initial condition by first defining a smooth slab on the surface and then allowing the slab to sink to the position shown in Figure 7a. A fine resolution mesh with a 129 × 129 grid is used, to mimic the trench-normal cross section. We compared the SBI first guess (Figure 7c) and the recovered solution (Figure 7d) through the same model that generates the reference states, with residual curves shown in Figure 7e. The SBI first guess is visually diffused while the recovered solution is nearly identical to the reference initial. Moreover, the dynamic topography associated with the SBI deviates from the reference by about 20% at 36 Ma while that with the recovered solution is less than 1%. This indicates that the recovered initial condition with simple forward adjoint looping is almost perfect if the viscosity and temperature scaling are known a priori.

[59] Since the inner level involving the forward-adjoint looping has been described in section 4.1, we focus our discussion on the middle and outer levels. For the middle level, we show several cases with different ΔT values,

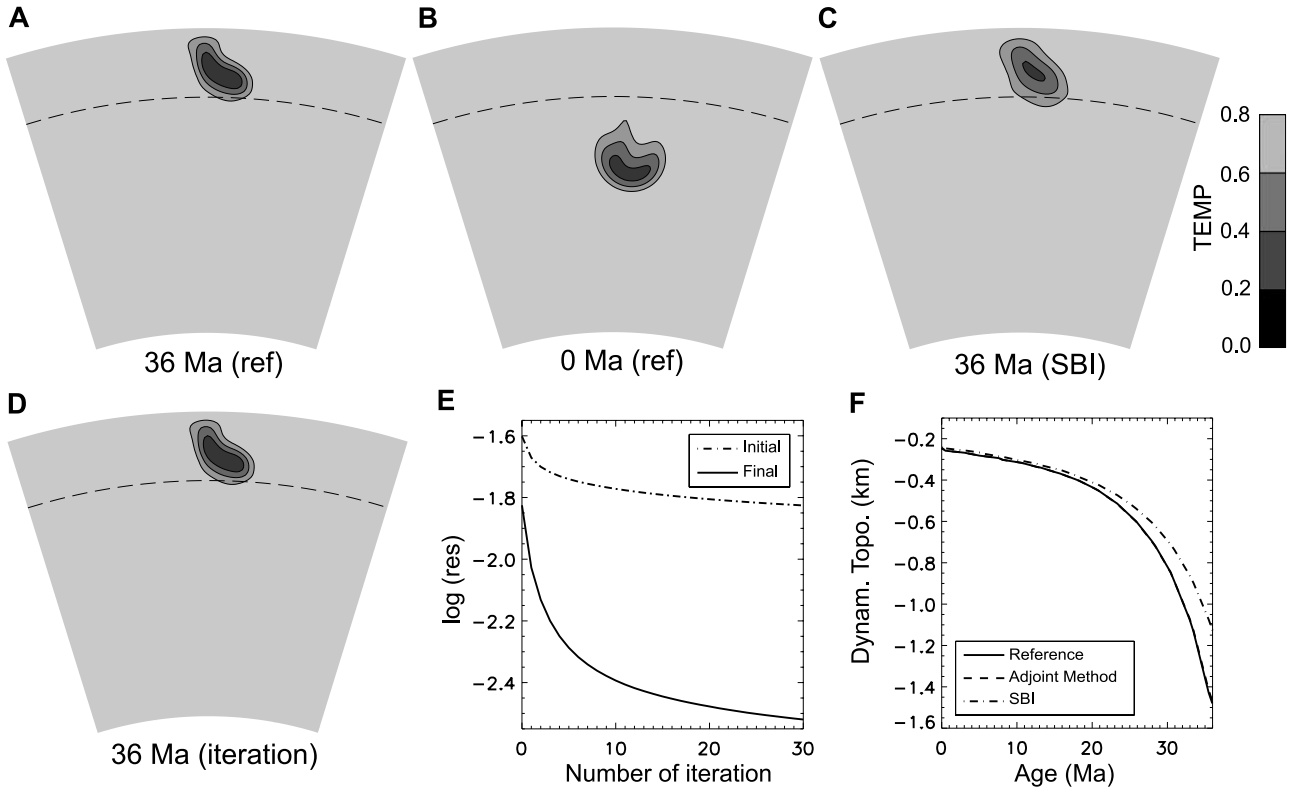

Figure 7. Same as Figure 5 except for 2-D models (on a 129 × 129 mesh) with a two-layer viscosity. (a–d) The dashed lines indicate the upper and lower mantle interface.

where upper and lower mantle viscosities are recovered from several initial guesses.

[60] In a set of experiments, we chose ΔT at its reference value but incorrectly guessed both viscosities. We tried two starting viscosity models AH3 and AH4 that were both guessed to be isoviscous with (η_{um}, η_{lm}) = (5, 5) and (20, 20), respectively, while the target had a layered viscosity, (η_{um}, η_{lm}) = (1, 10) (Figures 8a and 8c). Because the initial upper/lower mantle viscosity ratio was overestimated in both models, equation (19) implies that the present-day dynamic topography should be over predicted, as verified as loop 1 in Figures 8b and 8d. Since η_{lm} was controlled by the magnitude of topography during the later part of its evolution, the over predicted magnitude of h caused η_{lm} to increase (Figures 8a and 8c). Since the upper mantle viscosity η_{um} was overestimated in both AH3 and AH4, the rate of the change of topography was small during the early stages of evolution (Figures 8b and 8d). This difference forced η_{um} to decrease quickly in both cases. Changes in both η_{um} and η_{lm} likewise reduced their ratio. As a result, in AH3, both viscosities changed monotonically (Figure 8a), while in AH4, η_{lm} first overshot the target (Figure 8c). This overshoot happened because η_{lm} was forced to increase at the beginning due to an initially overpredicted h, but as η_{um} decreased the viscosity ratio went below the reference, h became underpredicted which led to the final decrease of η_{lm}. As the viscosities converged, the topographic evolution conformed to the target in both cases after a finite number of loops (Figures 8b and 8d). We conclude that the solution is potentially robust as it does not depend on the initial models. Additional experiments demonstrate that solution errors of both upper and lower mantle viscosities are within 1%.

[61] With another set of experiments with all target values as those just described (AH3 and AH4), but we incorrectly guessed ΔT so that it was either smaller (AH5) or larger (AH6) than the true value by 50%. AH5 started with an initially isoviscous state, (η_{um}, η_{lm}) = (5, 5) (see Figure 9a loop 1); and AH6 started with a higher viscosity, (η_{um}, η_{lm}) = (20, 20) (see Figure 9c loop 1). The initial models were chosen such that their effective Rayleigh numbers were not too far from the target values. Parameter recovery in these two cases was similar to what we observed above. Although the viscosity ratio R_η was the same in both AH5 and AH6, the present-day dynamic topographies were different in loop 1, in proportion to the different temperature scaling ΔT (equation (19)). Consequently, lower mantle viscosities η_{lm} evolved very differently when the temperature was incorrectly guessed. In both cases AH5 and AH6, converged solutions for both viscosities and dynamic topography were obtained. However, although the recovered upper mantle viscosities were always close, there was a tradeoff between lower mantle viscosity and the temperature scaling, as expected from equation (19). With more tests on different initial viscosity models, we found that the solutions were robust in that the converged viscosities oscillated around some mean values by no more than 5%. Deviations of the topographic evolutions from the target are instructive (Figures 9b and 9d): due to the tradeoff between ΔT and η_{lm}, the later portion of the predicted curve (closer to

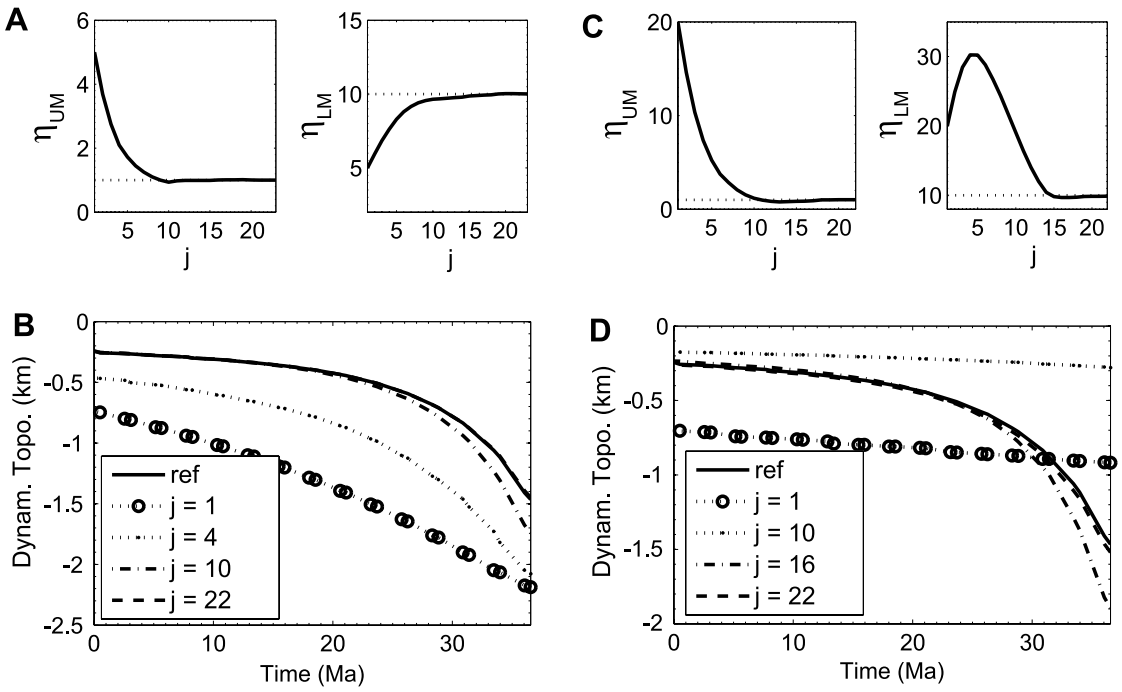

Figure 8. A two-level looping for recovery of both viscosities and initial condition, with temperature scaling at its reference value. Evolution of upper and lower mantle viscosities with respect to middle loop index (j) for cases (a) AH3 and (c) AH4, with dotted lines indicating the reference values. (b, d) Convergence of temporal dynamic topography recorded at one point for cases AH3 and AH4, respectively.

present-day) always matched the reference curve; however the early portion of the curves were never well predicted since ΔT did not trade off with η_{um}. Specifically, the earliest portion of the curve was flatter than the reference when ΔT was smaller, and steeper when ΔT larger.

[62] This deviation in topographies during the early part of evolution is the basis of an outer level iteration for the update of ΔT. When ΔT is incorrect, lower mantle viscosity trades off with temperature, upper mantle viscosity does not; in theory, dynamic topography can never be predicted

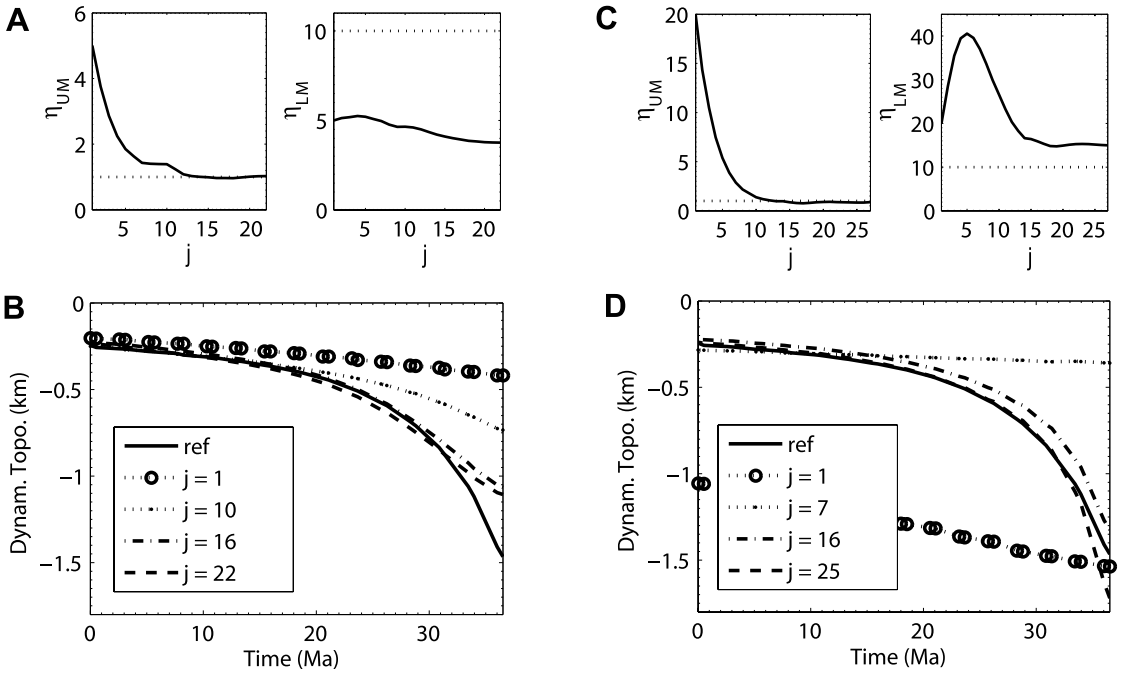

Figure 9. Same as Figure 8, except that the temperature scaling is either (a, b) smaller (case AH5) or (c, d) larger (case AH6) than the reference value by 50%.

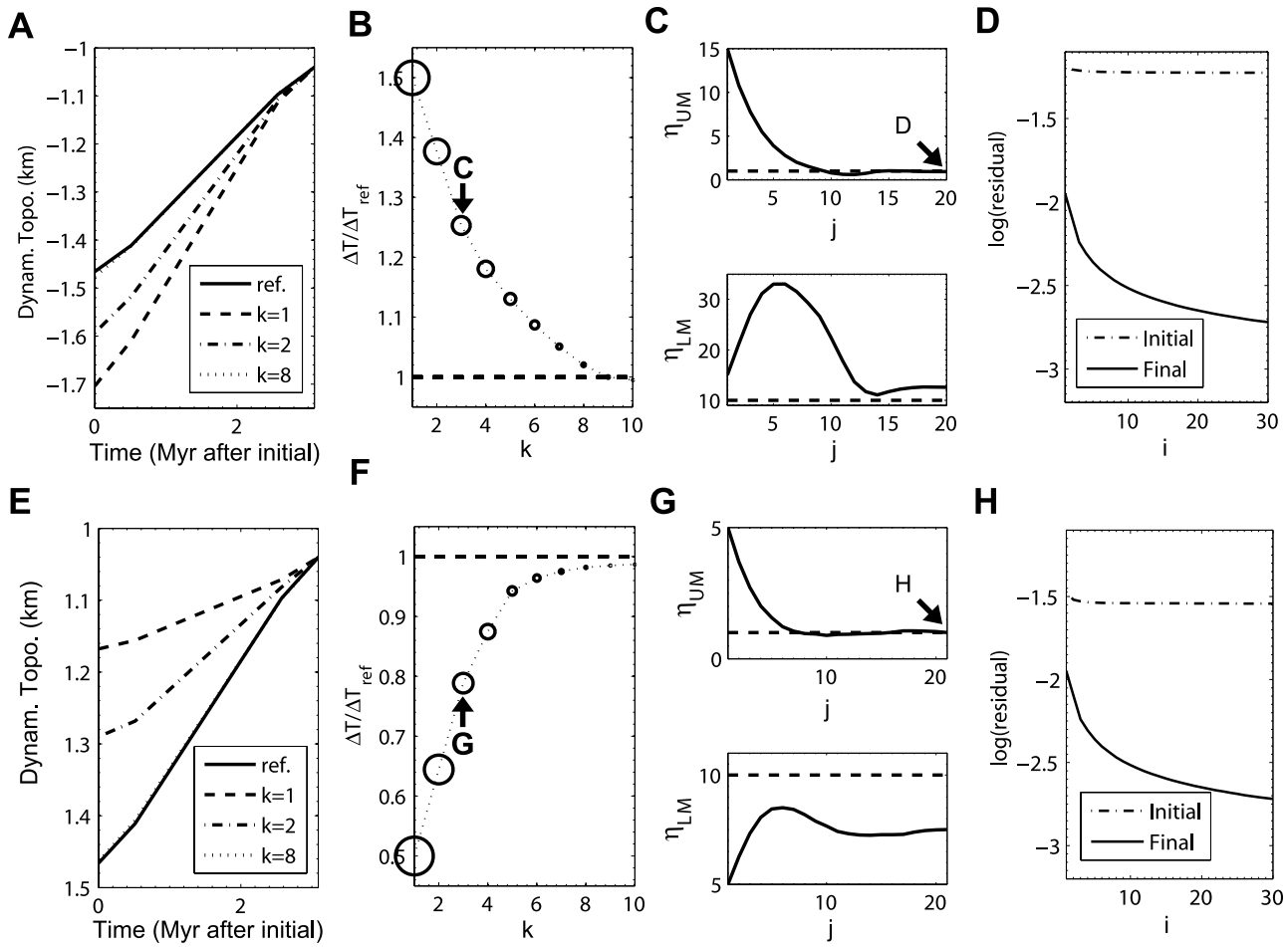

Figure 10. The three-level looping algorithm shown for cases (a–d) AHT1 and (e–h) AHT2, with i, j, and k denoting the index of inner, middle, and outer loops, respectively. Shown are evolution of topography at the earliest time (Figures 10a and 10e) and temperature scaling (Figures 10b and 10f) with respect to outer loop, convergence of upper and lower mantle viscosities versus middle loop, and RMS residuals for both initial and final states of temperature fields for chosen temperature scaling and viscosities. In Figures 10b and 10f, the size (area) of the open circles correspond to the mismatch between magnitudes of predicted and reference dynamic topography in Figures 10a and 10e, respectively. All dashed lines indicate the target values.

exactly if ΔT is incorrect. Equations (13) and (18) imply that different ΔT lead to different early topographic evolutions. In practice, we used the very simple relation described by equation (13) to update ΔT, constrained from the deviation described above. The iterative relation is given by equation (16), where n is the number of data points within the time period when this deviation occurred. Instead of using the absolute magnitude of dynamic topography, we used the amount of change of topography from the initial time to the nth point. Essentially, we use the difference in the slope at the initial stage of subduction.

[63] As an example, we used the values of ΔT in AH5 and AH6 as two starting guesses for the temperature scaling and then applied an additional outer loop (calling these new cases, AHT1 and AHT2). The procedure for the outer loop is described above. Note that with different values of ΔT, the converged dynamic topography had different slopes at initial times. We calculated the mismatch between the predicted and reference dynamic topography over the early part of topographic evolution and applied equation (16) to update ΔT. Consequently, the deviated topographic curves in both AHT1 (Figure 10a) and AHT2 (Figure 10e) moved toward the reference as the number of outer loops increased. Convergence of ΔT were shown in Figures 10b and 10f with respect to outer loop, where the symbol size was proportional to the residual between predicted and reference dynamic topography. Both the evolution of topography and that of ΔT indicated a correct convergence. To show the interior process of this three-level looping scheme, we picked some value of ΔT during the evolution as an example. For this ΔT, we plotted the updating mantle viscosities, i.e., the middle level loop (Figures 10c and 10g). The inner most loop was shown for the two converged viscosities where the RMS residuals between predicted and target mantle thermal structure at the initial and final (present-day) time were plotted (Figures 10d and 10h). These experiments illustrate well that when ΔT is incorrect, recovered η_{lm} is also incorrect; recovered mantle initial

conditions based on these model parameters are far from the reference initial since the RMS residuals remain large (compare Figures 10d and 10h with Figure 7e). By fitting the slope of the topography (Figures 10a and 10e), ΔT was constrained to converge. The recovered temperature scaling in both cases approximated its target value within 1%. How closely the final solution fits will be affected by the discretization of data and the form of weighting functions in equations (16), (20), and (21). In the final solution, all recovered model parameters have errors less than 1%, where the lower mantle viscosity linearly trades off with temperature scaling.

[64] In summary, our experiments show that, given a record of dynamic topography and the present-day mantle seismic tomography, this three-level looping scheme allows the recovery of all three parameters.

5. Discussion and Conclusions

[65] Constraining the state of the mantle in the past (i.e., initial conditions) is essential for geodynamic studies of plate motion [e.g., *Lithgow-Bertelloni and Richards*, 1998], hot spot drift [e.g., *Steinberger and O'Connell*, 2000], and sea level change [e.g., *Gurnis et al.*, 1998]. These three kinds of studies linking observations (plate motions, hot spot tracks, and continental stratigraphy) to geodynamic models all employed estimates of initial conditions based on different methods that we will describe below. However, to infer initial conditions none of these geodynamic studies used adjoint methods widely developed for atmospheric and oceanographic problems. In order to better constrain mantle initial conditions and properties, we continued development of adjoint and inverse methods for mantle convection.

[66] Inferring initial conditions with adjoint methods for mantle convection seems inherently ambiguous compared to atmospheric circulation problems where direct constraints on initial conditions from measurements in the system interior are used. Using a technique similar to that in the work of *Bunge et al.* [2003], we first inferred initial conditions via the looping between forward and adjoint calculations to minimize the difference between a prediction and the final state of the mantle (a state that can be determined from seismic tomography). An optimal convergence requires some preconstraint on the initial condition. Starting the first forward calculation with an isothermal mantle was less efficient than with an initial guess obtained by the simple backward integration (SBI) of the convection equations that starts with present-day structure.

[67] The adjoint method is an iterative gradient method that solves for a linearized problem. For the final solution to reach the global minimum in the residual space, the trial solution in the first iteration must be close to the true solution. Since the SBI initial guess makes use of present-day mantle information, this inverse of mantle convection approximates the true solution to first order. Therefore, the SBI initial guess guarantees a good solution with the adjoint method, as long as the model has not been run so long that diffusion at boundary layers dominates the problem.

[68] The SBI initial guess is close to optimal for most mantle convection problems because advection dominates thermal diffusion with a typical Peclet number on the order of 10^3. To best approximate the true solution, an initial guess must capture its total buoyancy and geometry that we demonstrated with several numerical experiments in which either the buoyancy was underestimated or the initial location was incorrect. In these cases, the trial solutions all have large initial errors that must be iteratively removed with forward adjoint looping. An idealized case with the correct initial location and buoyancy that is close to the actual initial condition recovers the initial condition nearly as well as the SBI. Since the SBI involves the solution of the three conservation equations (equations (2)–(4)), we obtain a condition that has almost the same total buoyancy as that in the true solution and with its geometry defined through the coupled solution of flow and advection; this initial guess will, of course, lead to a good solution. It is worthwhile to note that, even for a thermal boundary layer problem where diffusion dominates; this SBI initial guess still seems to be preferred [*Ismail-Zadeh et al.*, 2001].

[69] Even when a Stokes sphere interacts with and distorts a thermal boundary layer, where diffusion is important, the SBI continues to provide a good first guess. However, SBI will face difficulty when the anomalies reach a thermal boundary layer (TBL) and gradually diffuse away, which means SBI will not provide the same amount of buoyancy force. This is the natural limit for the adjoint method [*Ismail-Zadeh et al.*, 2004].

[70] Seismology has revealed that the mantle has both seismically fast and slow regions that putatively represent a complex combination of thermal and chemical anomalies [*Masters et al.*, 2000; *Ishii and Tromp*, 1999; *Ni et al.*, 2002]. In these real cases where mantle anomalies have irregular geometry and amplitude, arbitrary initial guesses can hardly capture the true solution in the first place, and the SBI initial guess will be especially beneficial.

[71] Combined with dynamic topography observations, the application of the adjoint method can be expanded so that not only can past mantle structures be recovered but constraints placed on mantle properties. On the basis of the governing equations, we developed multilevel iteration schemes that constrain both mantle thermal anomalies (the scaling between seismic velocity and temperature or density) and absolute values of upper and lower mantle viscosities. With synthetic experiments, we show that our algorithm is stable and robust. It is worthwhile to note that although this algorithm allows all three model parameters to vary while the final solution remains unique (the uniqueness depends on the recovering power of the adjoint method), in practice we should take advantage of a priori knowledge of these quantities, which will reduce the calculation time substantially. This will be essential for large 3-D models.

[72] Synthetic experiments are ideal, and realistic modeling is limited by other factors, including the availability and quality of data. Dynamic topography can be spatially and temporally incomplete, but a complete record is not required for convergence. For example, the dynamic topography constraints on Australian vertical motion since the Cretcaeous are limited to specific intervals of time [*Gurnis et al.*, 1998; DiCaprio et al., submitted manuscript, 2008]. Rate of change of dynamic topography associated with upper mantle thermal structures is especially useful and requires better data coverage both in time and in space, which also seems to be the case in reality [*Pang and Nummedal*, 1995; *Bond*, 1979]. Given these features, our method may work well

when applied to realistic modeling problems, for example, reconstructing the subduction history of the Farallon plate underneath North America, using the stratigraphic record on the continent of North America and tomographic image under the continent. Errors associated with recovered dynamic topography from stratigraphy will propagate into the solution of lower mantle viscosity and temperature scaling, mainly due to the fact that these two quantities strongly trade off.

[73] The physical significance of this study is twofold. First, it is a new way to calculate mantle viscosities which is almost perfect in synthetic tests as discussed in this paper. This method has an equally good recovery of both upper and lower mantle viscosity, not like glacial rebound models sampling mostly the upper mantle. Furthermore, our methods put constraints on the absolute viscosities of the mantle, while previous geoid studies constrain the upper–lower mantle viscosity ratio only. Second, when using real data including seismic tomography, the constraint on the temperature to velocity scaling by this method can be important for understanding the relation between seismic velocities and temperature and pressure under mantle conditions.

[74] The inherent power of our inverse method is that a single density anomaly rises (sinks) through the whole mantle and at each depth samples the viscosity through the rate at which dynamic topography changes. Inherent in this idea is that the magnitude of the density anomaly remains fixed. Of course, the assumption of a constant density difference at each depth is unlikely to be true for mantle convection because the mantle is compressible and different materials will compress at different rates as they ascend (descend) through the mantle [e.g., *Tan and Gurnis*, 2007].

[75] The recovery of initial conditions, two viscosities, and the temperature scaling, from only dynamic topography and the shape of the present-day temperature structure (i.e., "seismic tomography") appears to be under determined. However, for the synthetic experiments this is not the case. The reason is that we have a set of dynamic topography values: one value of dynamic topography places some constraints on the temperature scaling while two dynamic topographies early in the evolution constrain the shallow viscosity (for example), while two dynamic topographies later in the evolution constrain the deeper viscosity. Together, the set of data leads to the recovery of the viscosities, temperature scaling, and initial condition. However, in reality the problem is likely to be underdetermined because the number of unique dynamic topography values will be limited and the mantle presumably has a more complex viscosity structure than simulated by a two-layer model.

[76] We should point out that the relationships we developed between different model parameters and the looping schemes we employed are not the only forms as other constraints not considered here could be added to the time-dependent problem (such as the present-day geoid and the history of plate motions).

[77] Another issue for problems tailored to the observational record is plate motions, which are an important constraint on mantle flow [e.g., *Hager and O'Connell*, 1979]. When dynamic topography is used in the inverse procedure, plate motions complicate the problem since the stratigraphic record moves with respect to the rising and sinking mantle anomalies [*Gurnis et al.*, 1998]. Therefore, a transfer function between the two reference frames is needed. The means to overcome this complication is now underway.

[78] The use of tomography-based adjoint methods is not the only way to infer the internal state of the mantle at earlier times and we suggest that there are two other means to arrive at such "initial conditions." In plate motion constrained mantle flow models, mantle structures can be estimated by a "forward approach" in which a flow model is started earlier in time and then integrated forward to the time of interest [*Bunge et al.*, 1998, 2002]. Initial conditions can also be inferred via a tectonic approach based on generating the internal state at a previous time from some combination of surface observations (such as proxies for the configuration of plates, the position of subduction, or hot spot volcanism). For example, based on the orientation of Mesozoic subduction, *Gurnis et al.* [1998] developed an initial condition at 130 Ma and then forward simulated convection beneath Australia. *Bunge and Grand* [2000] used the geological arguments that the Farallon slab was flat lying at ~80 Ma and then forward modeled flow beneath North America. These methods complement the inverse models and have different sources of errors. The forward and inverse approaches shared two sources of error: subduction parameterization and radial viscosity structure. However, forward models were sensitive to uncertainties in the plate reconstruction further back in time while inverse models were sensitive to error in reconstructions from the time of interest to the present. We suspect that uncertainty (e.g., the range of structural models permissible at any given time) can be better estimated by comparing the results from these three different methods of generating paleomantle structures. Consequently, we believe that the adjoint and inverse methods we have developed here should be used in conjunction with the forward and tectonic approaches. Together, these methods will allow a new generation of global and dynamic models to be developed that have well constrained initial conditions.

[79] **Acknowledgments.** We thank Malcolm Sambridge for numerous discussions on inverse methods. The original CitcomS software was obtained from CIG, Computational Infrastructure for Geodynamics (http://geodynamics.org). This is contribution 8998 of the Division of Geological and Planetary Sciences and 78 of the Tectonics Observatory, Caltech. All calculations carried out on the Caltech Geosciences Supercomputer Facility partially -supported by NSF EAR-0521699. Additional support provided through the Caltech Tectonics Observatory by the Gordon and Betty Moore Foundation.

References

Bond, G. C. (1979), Evidence for some uplifts of large magnitude in continental platforms, *Tectonophysics*, *61*, 285–305, doi:10.1016/0040-1951(79)90302-0.

Bunge, H.-P., and S. P. Grand (2000), Mesozoic plate-motion history below the northeast Pacific Ocean from seismic images of the subducted Farallon slab, *Nature*, *405*, 337–340, doi:10.1038/35012586.

Bunge, H.-P., M. A. Richards, C. Lithgow-Bertelloni, J. R. Baumgardner, S. P. Grand, and B. A. Romanowicz (1998), Time scales and heterogeneous structure in geodynamic Earth models, *Science*, *280*, 91–95, doi:10.1126/science.280.5360.91.

Bunge, H.-P., M. A. Richards, and J. R. Baumgardner (2002), Mantle-circulation models with sequential data assimilation: Inferring present-day mantle structure from plate-motion histories, *Phil. Trans. R. Soc. London, Ser. A*, *360*, 2545–2567, doi:10.1098/rsta.2002.1080.

Bunge, H.-P., C. R. Hagelberg, and B. J. Travis (2003), Mantle circulation models with variational data assimilation: Inferring past mantle flow and structure from plate motions histories and seismic tomography, *Geophys. J. Int.*, *152*, 280–301, doi:10.1046/j.1365-246X.2003.01823.x.

Conrad, C. P., and M. Gurnis (2003), Seismic tomography, surface uplift, and the breakup of Gonwanaland: Integrating mantle convection backwards in time, *Geochem. Geophys. Geosyst.*, *4*(3), 1031, doi:10.1029/2001GC000299.

Cross, T. A., and R. H. Pilger (1978), Tectonic controls of Late Cretaceous sedimentation, western interior, USA, *Nature*, *274*, 653–657, doi:10.1038/274653a0.

Grand, S. P., R. D. van der Hilst, and S. Widiyantoro (1997), Global seismic tomography: A snapshot of convection in the Earth, *GSA Today*, *7*, 1–7.

Gurnis, M. (1993), Phanerozoic marine inundation of continents driven by dynamic topography above subducting slabs, *Nature*, *364*, 589–593, doi:10.1038/364589a0.

Gurnis, M., R. D. Müller, and L. Moresi (1998), Dynamics of Cretaceous vertical motion of Australia and the Australian-Antarctic discordance, *Science*, *279*, 1499–1504, doi:10.1126/science.279.5356.1499.

Gurnis, M., J. X. Mitravica, J. Ritsema, and H.-J. van Heijst (2000), Constraining mantle density structure using geological evidence of surface uplift rates: The case of the African Superplume, *Geochem. Geophys. Geosyst.*, *1*(7), 1020, doi:10.1029/1999GC000035.

Hager, B. (1984), Subducted slabs and the geoid: Constraints on mantle rheology and flow, *J. Geophys. Res.*, *89*(B7), 6003–6015, doi:10.1029/JB089iB07p06003.

Hager, B., and R. Clayton (1988), Constraints on the structure of mantle convection using seismic observations, flow models, and the geoid, in *Mantle Convection*, edited by W. R. Peltier, pp. 657–763, Gordon and Breach, New York.

Hager, B. H., and R. J. O'Connell (1979), Kinematic models of large-scale flow in Earth's mantle, *J. Geophys. Res.*, *84*, 1031–1048.

Huang, J., and D. Zhao (2006), High-resolution mantle tomography of China and surrounding regions, *J. Geophys. Res.*, *111*, B09305, doi:10.1029/2005JB004066.

Ishii, M., and J. Tromp (1999), Normal-mode and free-air gravity constraints on lateral variations in velocity and density of Earth's mantle, *Science*, *285*, 1231–1236, doi:10.1126/science.285.5431.1231.

Ismail-Zadeh, A. T., C. J. Talbot, and Y. A. Volozh (2001), Dynamic restoration of profiles across diapiric salt structures: Numerical approach and its applications, *Tectonophysics*, *337*, 23–38, doi:10.1016/S0040-1951(01)00111-1.

Ismail-Zadeh, A., G. Schubert, I. Tsepelev, and A. Korotkii (2004), Inverse problem of thermal convection: Numerical approach and application to mantle plume restoration, *Phys Earth Planet Inter.*, *145*, 99–114, doi:10.1016/j.pepi.2004.03.006.

Lithgow-Bertelloni, C., and M. A. Richards (1998), The dynamics of Cenozoic and Mesozoic plate motions, *Rev. Geophys.*, *36*, 27–78, doi:10.1029/97RG02282.

Masters, G., G. Laske, H. Bolton, and A. Dziewonski (2000), The relative behavior of shear velocity, bulk sound speed, and compressional velocity in the mantle: Implications for chemical and thermal structure, in *Earth's Deep Interior: Mineral Physics and Tomography From the Atomic to the Global Scale*, *Geophys. Monogr. Ser.*, vol. 117, edited by S. Karato et al., pp. 63–87, AGU, Washington, D.C.

Mitrovica, J., and A. Forte (1997), Radial profile of mantle viscosity: Results from the joint inversion of convection and glacial rebound observables, *J. Geophys. Res.*, *102*, 2751–2769, doi:10.1029/96JB03175.

Mitrovica, J. X., and A. M. Forte (2004), A new inference of mantle viscosity based upon joint inversion of convection and glacial isostatic adjustment data, *Earth Planet. Sci. Lett.*, *225*, 177–189, doi:10.1016/j.epsl.2004.06.005.

Montelli, R., G. Nulet, F. Dahlen, G. Masters, E. R. Engdahl, and S.-H. Hung (2004), Finite-frequency tomography reveals a variety of plumes in the mantle, *Science*, *303*, 338–343, doi:10.1126/science.1092485.

Ni, S., E. Tan, M. Gurnis, and D. Helmberger (2002), Sharp sides to the African superplume, *Science*, *296*, 1850–1852, doi:10.1126/science.1070698.

Pang, M., and D. Nummedal (1995), Flexural subsidence and basement tectonics of the Cretaceous Western Interior basin, United States, *Geology*, *23*, 173–176.

Richards, M., and B. Hager (1984), Geoid anomalies in a dynamic earth, *J. Geophys. Res.*, *89*, 5987–6002, doi:10.1029/JB089iB07p05987.

Ritsema, J., H. J. van Heijst, and J. H. Woodhouse (2004), Global transition zone tomography, *J. Geophys. Res.*, *109*, B02302, doi:10.1029/2003JB002610.

Rowlinson, N., and M. Sambridge (2003), Seismic traveltime tomography of the crust and lithosphere, *Adv. Geophys.*, *46*, 181–197.

Sandiford, M. (2007), The tilting continent: A new constraint on the dynamic topographic field from Australia, *Earth Planet. Sci. Lett.*, *261*, 152–163, doi:10.1016/j.epsl.2007.06.023.

Sirkes, Z., and E. Tziperman (1997), Finite difference of adjoint or adjoint of finite difference?, *Bull. Am. Meteorol. Soc.*, *125*, 3373–3378.

Steinberger, B., and R. O'Connell (2000), Effects of mantle flow on hotspot motion, in *The History of Dynamics of Global Plate Motion*, *Geophys. Monogr. Ser.*, vol. 121, edited by M. A. Richards, R. G. Gordon and R. D. van der Hilst, pp. 377–398, AGU, Washington, D. C.

Sun, J., D. W. Flicker, and D. K. Lilly (1991), Recovery of 3D wind and temperature fields from simulate single-Doppler radar data, *J. Atmos. Sci.*, *48*(6), 876–890.

Talagrand, O., and P. Courtier (1987), Variational assimilation of meteorological observation with the adjoint vorticity equation, *Q. J. R. Meteorol. Soc.*, *113*, 1311–1328, doi:10.1256/smsqj.47811.

Tan, E., and M. Gurnis (2007), Compressible thermochemical convection and application to lower mantle structures, *J. Geophys. Res.*, *112*, B06304, doi:10.1029/2006JB004505.

Tan, E., E. Choi, P. Thoutireddy, M. Gurnis, and M. Aivazis (2006), GeoFramework: Coupling multiple models of mantle convection within a computational framework, *Geochem. Geophys. Geosyst.*, *7*, Q06001, doi:10.1029/2005GC001155.

Tarantola, A. (2005), *Inverse Problem Theory and Methods for Model Parameter Estimation*, Soc. for Ind. and Appl. Math., Philadelphia, Pa.

Van der Hilst, R. D., S. Widiyantoro, and E. R. Engdahl (1997), Evidence of deep mantle circulation from global tomography, *Nature*, *386*, 578–584, doi:10.1038/386578a0.

Walcott, R. (1973), Structure of the Earth from glacio-isostatic rebound, *Annu. Rev. Earth. Planet. Sci.*, *1*, 15–37.

Zhao, D., X. Xu, D. A. Wiens, L. Dorman, J. Hildebrand, and W. Webb (1997), Depth extent of the Lau back-arc spreading center and its relation to subduction processes, *Science*, *278*, 254–257, doi:10.1126/science.278.5336.254.

Zhong, S., M. T. Zuber, L. Moresi, and M. Gurnis (2000), The role of temperature-dependent viscosity and surface plates in spherical shell models of mantle convection, *J. Geophys. Res.*, *105*, 11,063–11,082, doi:10.1029/2000JB900003.

M. Gurnis and L. Liu, Seismological Laboratory, California Institute of Technology, Pasadena, CA 91125, USA. (lijun@gps.caltech.edu)